NOAA Technical Memorandum ERL ETL-265

THE POTENTIAL OF 8-MM-RADARS FOR REMOTELY SENSING CLOUD DROP-SIZE DISTRIBUTIONS

E.E. Gossard
J.B. Snider
B.E. Martner
J.S. Gibson
A.S. Frisch
R.A. Kropfli

Environmental Technology Laboratory
Boulder, Colorado
March 1996

noaa NATIONAL OCEANIC AND ATMOSPHERIC ADMINISTRATION / Environmental Research Laboratories

NOAA Technical Memorandum ERL ETL-265

THE POTENTIAL OF 8-MM-RADARS FOR REMOTELY SENSING CLOUD DROP-SIZE DISTRIBUTIONS

E.E. Gossard
J.B. Snider
Cooperative Institute for Research in Environmental Sciences (CIRES)

B.E. Martner
J.S. Gibson
A.S. Frisch
R.A. Kropfli
Environmental Technology Laboratory

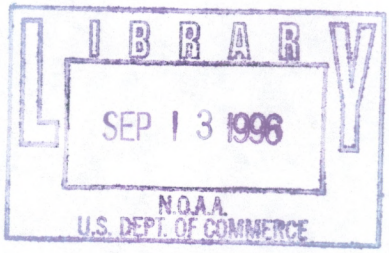

Environmental Technology Laboratory
Boulder, Colorado
March 1996

UNITED STATES
DEPARTMENT OF COMMERCE

Ronald H. Brown
Secretary

NATIONAL OCEANIC AND
ATMOSPHERIC ADMINISTRATION

D. JAMES BAKER
Under Secretary for Oceans
and Atmosphere/Administrator

Environmental Research
Laboratories

James L. Rasmussen
Director

NOTICE

Mention of a commercial company or product does not constitute an endorsement by NOAA/ERL. Use of information from this publication concerning proprietary products or the tests of such products for publicity or advertising purposes is not authorized.

For sale by the National Technical Information Service, 5285 Port Royal Road
Springfield, VA 22161

CONTENTS

The Potential of 8-mm Radars for Remotely Sensing Cloud Drop-Size Distributions

E. E. Gossard,[1] J. B. Snider,[1] B. E. Martner, J. S. Gibson, A. S. Frisch, and R. A. Kropfli

ABSTRACT. This paper describes the use of a vertically pointing 8.6-mm-wavelength Doppler radar for measuring drop-size spectra in clouds. The data used were collected in the Atlantic Stratocumulus Transition Experiment (ASTEX) in 1992. A radar technique for extracting information farther into the small-drop regime than previously attempted is described, and the amount of liquid residing in the cloud regime is compared with that found in the precipitation regime where drop fall velocities are resolvable. Total liquid is compared with that measured with a collocated three-channel microwave radiometer. Examples of number density spectra, liquid water spectra, and flux spectra are shown and compared with what is known of these quantities from various *in situ* measurements by aircraft in similar clouds. Error estimates and uncertainties are discussed. It is concluded that 8-mm Doppler radars have the potential for broader use in cloud and precipitation studies than generally realized.

1. INTRODUCTION

Vertically pointing measurements of a marine stratus cloud were obtained during the Atlantic Stratocumulus Transition Experiment (ASTEX) using the NOAA/Environmental Technology Laboratory's (ETL) 35-GHz (K_a-band) Doppler cloud research radar. This radar is especially well-suited for measurements of nonprecipitating and weakly precipitating cloud features by virtue of its excellent sensitivity (-30 dBZ at 10-km range), resolution (37.5-m pulse length, 0.5° beamwidth, and 0.25-s sample time), and accuracy (±5 cm s^{-1} under typical conditions). The short wavelength (8.6 mm) of this radar imparts an inherent sensitivity advantage over longer-wavelength radars for detection of the small hydrometeors that constitute clouds because the backscattering cross section of cloud droplets is proportional to λ^{-4} for Rayleigh scattering. Furthermore, the wavelength is sufficiently short that contributions to the observed reflectivity from clear-air, refractive-index, turbulent fluctuations are negligible compared with those from hydrometeors. Rainfall exceeding drizzle intensity, however, can cause attenuation of the signal at this wavelength. Attenuation from water vapor can also be significant for radars of shorter wavelength than this. Examples of the NOAA/ETL radar's ability to detect weak, fine-scale cloud features—and its use in deriving a variety of cloud microphysical parameters through the use of its Doppler moments measurements—are given by Martner and Kropfli (1993) and Kropfli et al. (1994). In this article, Doppler spectra, recorded in the radar's time-series mode with a height resolution of 150 m, are utilized.

---

[1]Cooperative Institute for Research in Environmental Sciences (CIRES), University of Colorado/NOAA, Boulder, Colorado 80309.

In the large-drop regime of liquid clouds, where fall velocities are much greater than the turbulent velocity, Doppler radar measurements generally agree well with *in situ* measurements by aircraft (e.g., Rogers et al. 1993). In this regime, the precipitation spectral domain is easily separated by fall velocity from the cloud (or clear-air) spectral domain that is typically used by wind profilers to measure winds. This peak, near zero fall velocity, is then used to remove up/ downdrafts in the medium, and the corrected fall velocity spectrum is converted to drop-size distribution (e.g., Atlas et al. 1973). In this regime, the reflectivity and fall velocity are the important measurables.

On the other hand, for small droplets the settling velocity (i.e., the terminal fall velocity of cloud droplets) is usually small compared with the turbulent velocity fluctuations in the medium. The droplets then serve mainly as tracers of the turbulent motion of the air, and their backscatter is not inherently distinguishable from the clear-air return. In this regime, the terminal fall velocity is not useful for deducing drop size. Turbulent movement of the droplets "smears" the fall velocity spectrum (Wakasugi et al. 1986, 1987; Gossard 1988; Gossard and Strauch 1990; Gossard et al. 1990; Sato et al. 1990; Currier et al. 1992; Rajopadhyaya et al. 1993; Gossard 1994), and the measured spectrum is, in fact, the convolution of the fall (settling) velocity with the turbulent velocity probability density function (PDF). Therefore, the measured spectrum must be deconvolved, and the spectral width (w_o) replaces V_f as the important radar measurable, as illustrated in Fig. 1, where downward velocities are positive. Figure 1 shows the normalized radar reflectivity spectrum from a hypothetical gamma droplet distribution in quiet air (solid, $w_o = 0$) compared with corresponding theoretical reflectivity spectra when the population is embedded in an atmosphere with various levels of turbulence (dashed). In this paper, we deal with a case of heavy stratus with some drizzle and deconvolve the measured spectra to recover the cloud spectrum and separate it from the drizzle regime. In this case, we find that the cloud and drizzle peaks are usually separable because of the very high spectral-velocity resolution (2.6 cm s^{-1}) in the radar spectra. [A 330-point Fast Fourier Transform (FFT) was used in the data reduction.]

2. THE DATA

The data analyzed in this report were collected on Porto Santo Island in the Madeiras on June 12, 1992, from a 3-min time series beginning at 2109 UTC. Height profiles of Doppler cloud spectra were collected about every 0.2 s, with 150-m height spacing, providing about 1000 profiles of cloud spectra in the 3-min interval. The radar characteristics are summarized in Table 1. For the radar's 0.5° beamwidth, it samples a volume of about 10^4 m^3 every 0.2 s in each 150 m of altitude. Each spectrum covers a number density range of at least seven orders of magnitude. Thus, short-wavelength radars provide a tool of great potential in studying and monitoring cloud microstructure. A three-channel microwave radiometer was collocated (~20-m separation) with the radar to provide total liquid water above the site. The channels are coupled into a common antenna with 2.5° beamwidth. The offset paraboloid antenna is inside a shelter viewing a reflector outside oriented at 45° so that it reflects zenith radiation into the antenna.

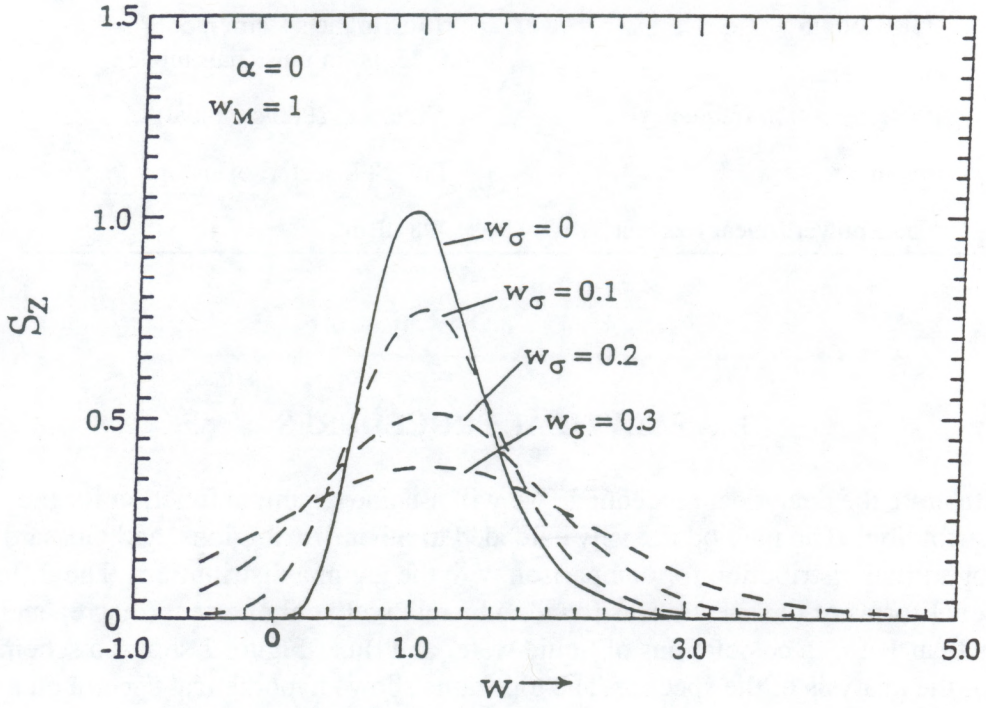

FIGURE 1. The effect of turbulent broadening on a fall velocity spectrum. The original spectrum unmodified by turbulence is the modified gamma function [see (7b), shown as the solid curve ($\alpha = 0$) in above figure]. Turbulence intensity is represented by w_σ, the half-width of a Gaussian PDF to the e^{-1} point, so the turbulent broadening for various intensities of turbulence is shown by the dashed curves. S_z is the reflectivity spectral density, and w is the fall velocity relative to its maximum (w_M).

TABLE 1. Characteristics of the K_a-band radar

Characteristic	Values
Antenna size	1.2 m
Beamwidth	0.5°
Maximum sidelobe	-30 dB relative to main
Wavelength	8.66 mm
Peak power	85 kW
Pulse length	1 μs (in the spectra mode) 0.25 μs (in pulse pair mode)
Pulse repetition frequency	Variable (2000/s typical)
Scanning	Full PPI, sector, over-top
Noise power (linear receiver)	-98 dBm

3. ANALYTICAL PROCEDURES

To illustrate the analytical procedures, we will assume a gamma function for the drop-size distribution. The method is easily extended to other distributions, and Gossard (1994) analyzed a lognormal distribution for comparison with the gamma distribution. The difference in the functional forms of the spectra was found to be relatively unimportant (discrepancies typically less than 10%) in calculations of liquid water and flux. Figure 2 shows a schematic description of the analysis of the spectra. The top frame shows hypothetical spectra on a log N_d plot, where N_d is drop-number density and D is drop diameter in millimeters. A gamma function is assumed for the drop-size distribution, so

$$N_d = N_0 D^{\alpha} e^{-\Lambda D} , \tag{1}$$

where α is an integer index. If $\alpha = 0$, then the distribution is the classical exponential. The figure shows two different exponential regimes for cloud and for precipitation. The radar reflectivity factor is

$$Z(D) = \int_{-\infty}^{\infty} N_d D^6 dD , \tag{2}$$

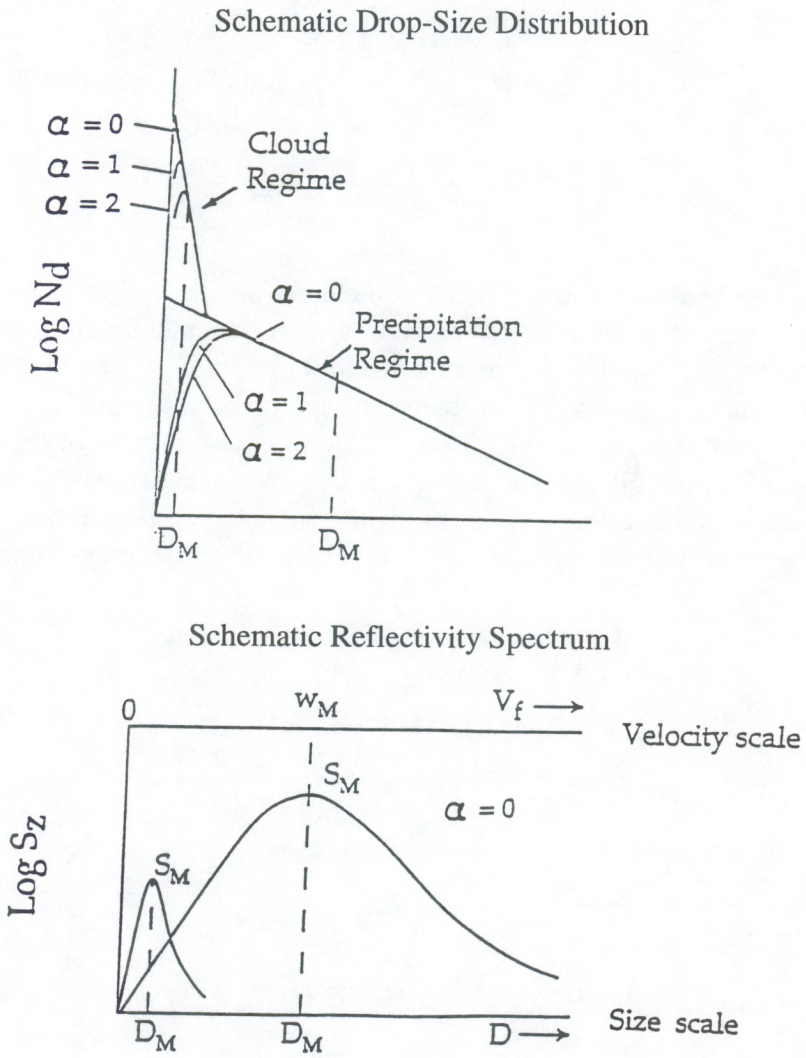

FIGURE 2. Top: Schematic picture of drop-number density spectra [see (1)] with a cloud regime (left) and a precipitation regime (right) for $\alpha = 0$, 1, and 2. For $\alpha = 0$, the distribution is exponential (straight line on log plot). Bottom: Corresponding reflectivity spectrum [see (3)] for $\alpha = 0$, showing how D_M and w_M are defined.

so the reflectivity spectrum is

$$S_z(D) = N_d D^6 \ . \tag{3}$$

The reflectivity spectra corresponding to the drop-size spectra in Fig. 2 (top) are shown in Fig. 2 (bottom).

Integrating (2) and using (1), we find [Gossard 1994, equation (24)] that

$$Z = S_{QM} w_M e^{(6+\alpha)} \frac{(6+\alpha)!}{(6+\alpha)^{(7+\alpha)}} = S_{QM} \frac{w_M}{f(\alpha)} \ , \tag{4}$$

where S_{QM} is the spectral maximum (subscript M) of the quiet-air (subscript Q) spectrum we seek. Equation (4) defines the function $f(\alpha)$ for future use. If the radar resolves the spectral peaks, we note that the reflectivity factor Z and the spectral maximum S_M are quantities that a radar measures well. Therefore, even in the presence of up/downdrafts, small w_M's can be deduced from (4). Because it depends on the *ratio* of Z to S, the calibration of the radar is not important to first order in deducing w_M (and, therefore, D_M). Note that D_M is defined as the size at the maximum or mode of the reflectivity spectrum and w_M is the corresponding vertical velocity. When the relationship between size and fall velocity is linear, they occur simultaneously.

The cloud liquid water, *LW*, is given by

$$LW = \int_{-\infty}^{\infty} M(D)\, dD = \rho_w(\pi/6) \frac{(6+\alpha)^3 (3+\alpha)!}{D_M^3 (6+\alpha)!} Z \ , \tag{5a}$$

where the liquid spectrum (g m^{-3} mm^{-1}) is

$$M(D) = \rho_w(\pi/6)\ N_d(D)\ D^3 \tag{5b}$$

and the flux, *FLX*, (g m^{-2} s^{-1}) is

$$FLX = \int_{-\infty}^{\infty} M(D)\, w(D)\, dD = \rho_w(\pi/6)\ w_M \frac{(6+\alpha)^2\ (4+\alpha)!}{D_M^3\ (6+\alpha)!} Z \ . \tag{6}$$

(If D_M is in millimeters or micrometers, the units of ρ_w must be suitably chosen to retain the proper units of M and ρ_w.)

We note that the radar measures S_M, whereas it is the quiet-air value, S_{QM}, that appears in (4). To get the quiet-air spectrum, the measured spectrum and the turbulent velocity PDF must be deconvolved. The procedure is described by Gossard (1994). We will assume that S_{QM} has the form of the gamma function. The integral to be solved is

$$S_z(w_i) = \frac{1}{\sqrt{\pi}\, w_\sigma^2} \int_0^\infty S_Q\left[D_j(w_j)\right] e^{\left[-(w_i - w_j)^2 / w_\sigma^2\right]} dw_j \,, \tag{7a}$$

where

$$S_Q(D_j) = S_{QA} \left[\frac{D_j}{D_M}\right]^{(6+\alpha)} e^{\left[(6+\alpha)(1 - D_j/D_M)\right]} \,, \tag{7b}$$

$$w_j = 4\,(\rho/\rho_0)^{-0.5}\, D_j \qquad \text{for the linear range of } V_f \text{ vs } D \,, \tag{7c}$$

$$w_j = 4\,(\rho/\rho_0)^{-0.5}\, D_j \left[1 - e^{-12 D_j}\right] \qquad \text{for interpolation to the Stokes range.} \tag{7d}$$

D_M is related to w_M by relations similar to (7c) and (7d), where D_M is the drop diameter at the maximum of the function (7b) and w_M is the corresponding vertical velocity. If w_M is the given quantity, S_M is calculated using (7c) or the implicit solution of (7d). The integrations are then best carried out numerically. The diagrams given in Gossard (1994) were not detailed or accurate enough at small-drop diameters for the cloud stratus case studied here, so they are replotted as the diagrams in Figs. 3–6 with many values of w_σ in the range of small w_M. Note that in the limit of very small drops, as V_f goes to zero, the deconvolved distribution tends to the PDF. If the PDF is Gaussian, Z/S_M is just $\pi^{0.5}\, w_\sigma$. Instead of plotting the deconvolution factor, DF, as in Gossard (1994), we plot DF^{-1} for convenience in interpolating graphical points.

The diagrams show that the size information is essentially lost for sizes smaller than $D_M = 0.04$ mm. In fact, when the interpolation equation (7d) is used, the solution is double-valued for very small diameters. (The more commonly used median diameter, D_0, is (3.67/6) $D_M = 0.024$ mm for $\alpha = 0$.) When the size D_M calculated from the observed Z_c/S_{MC} is smaller than 0.04 mm, we have used 0.04 mm when calculating cloud liquid. This yields a minimum value because smaller droplet populations have greater liquid for the same reflectivity. Only gates 5 and 6 had modal sizes greater than 0.04 mm, so the median radius of the cloud regime was typically less than 0.012 mm.

The analysis procedure is shown in Fig. 7. It shows the Doppler spectrum from gate 5 of the first averaged profile. It is chosen for illustration because the cloud and precipitation domains of the spectrum are well-defined and clearly separable. The first raw spectrum is shown beside it for comparison. Note that the separation of the regimes is clearly evident even in the raw spectra.

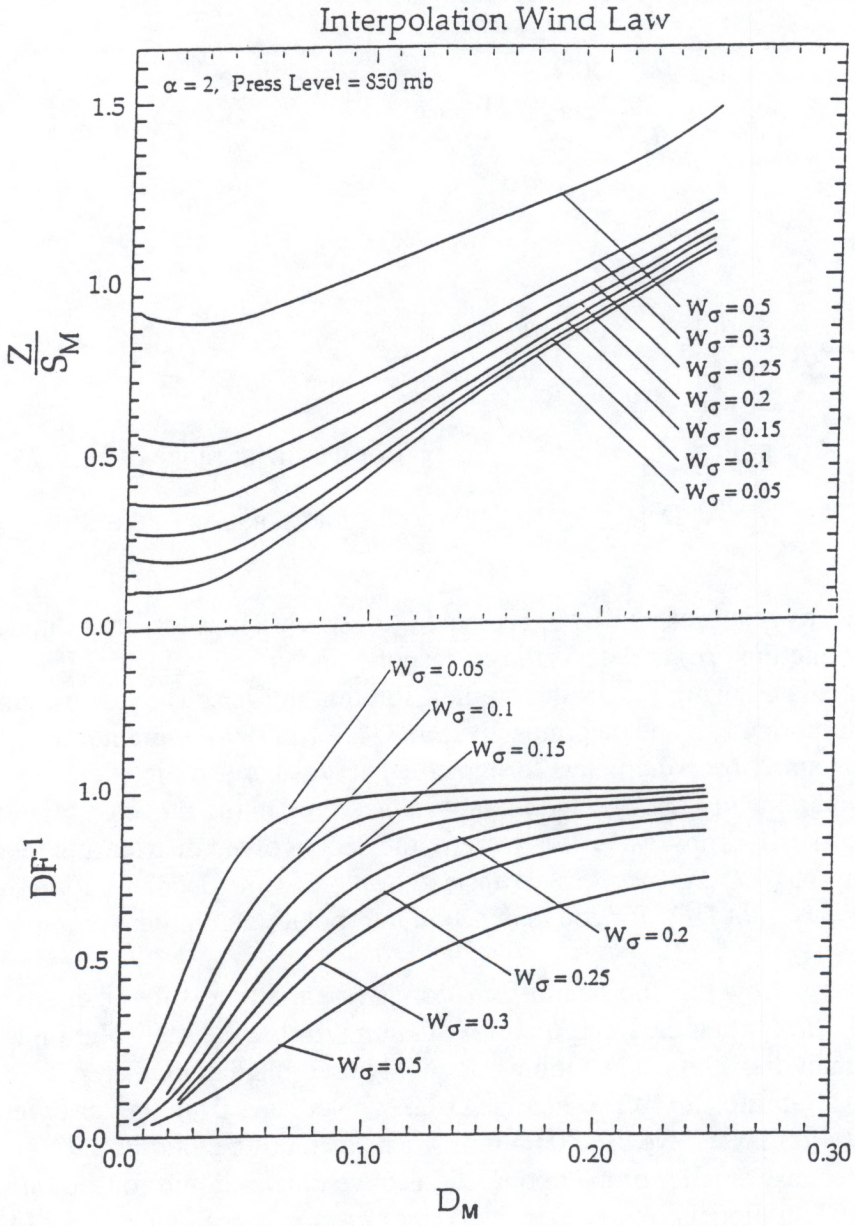

FIGURE 3. Top: Ratio of Z/S_M vs D_M for various turbulence intensities (w_σ), for the wind law indicated at the top of the figure, and the value of α shown in the upper left-hand corner. Bottom: The corresponding inverse magnitude of DF, plotted as its inverse for easy interpolation.

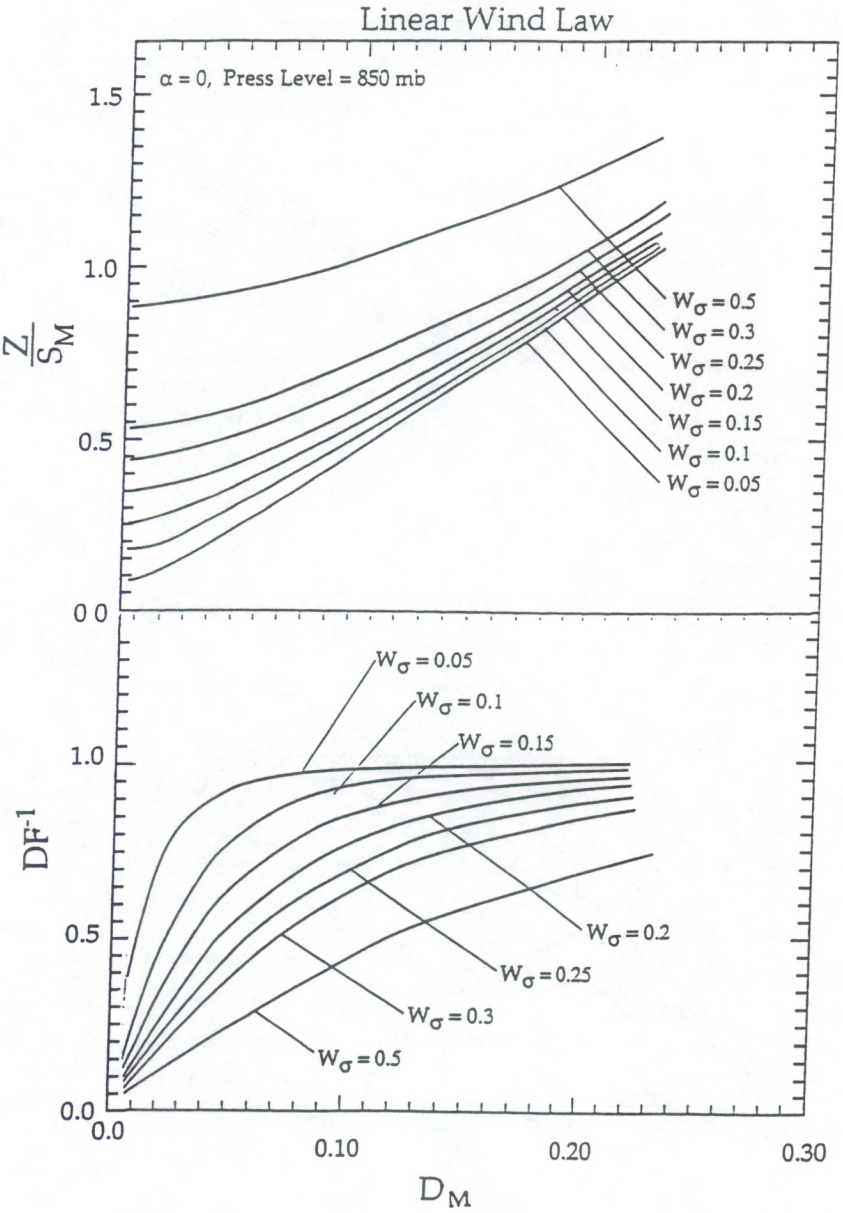

FIGURE 4. Top: Ratio of Z/S_M vs D_M for various turbulence intensities (w_σ), for the wind law indicated at the top of the figure, and the value of α shown in the upper left-hand corner. Bottom: The corresponding inverse magnitude of DF, plotted as its inverse for easy interpolation.

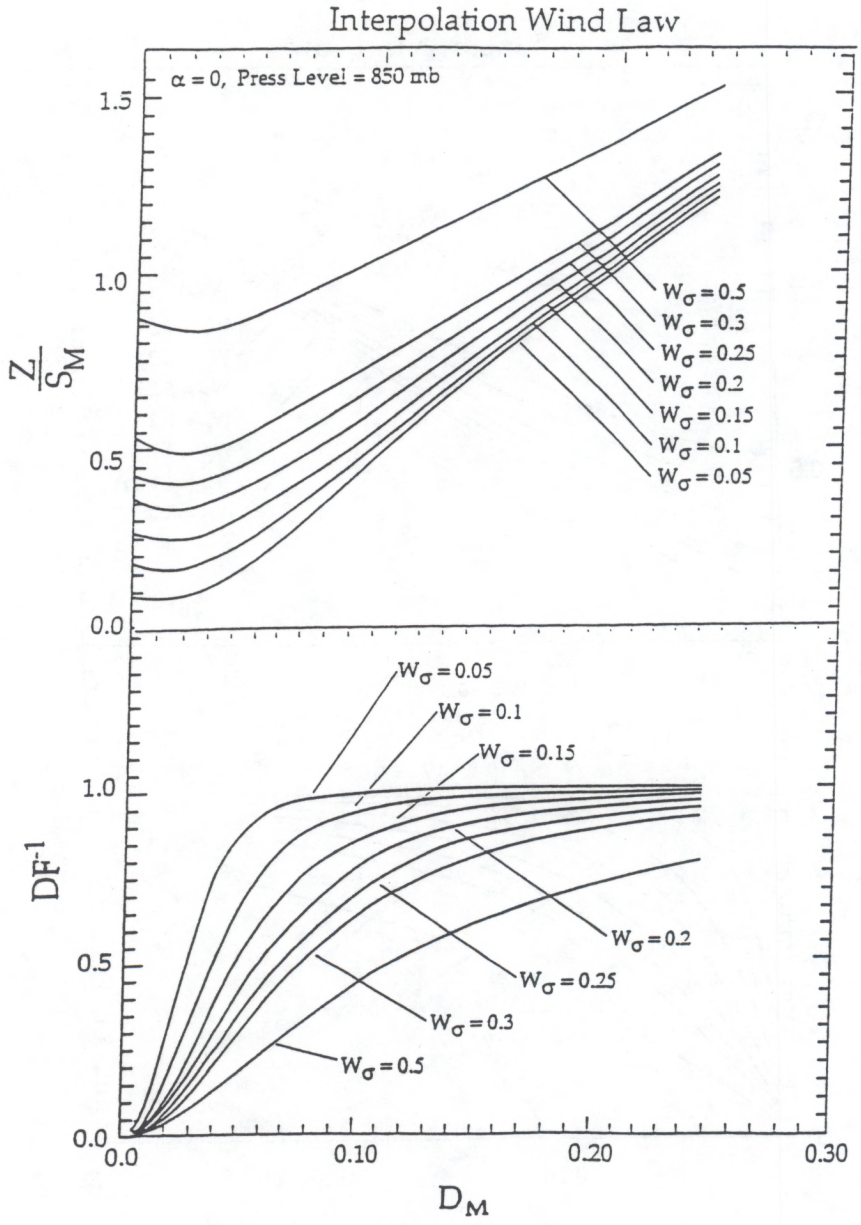

FIGURE 5. Top: Ratio of Z/S_M vs D_M for various turbulence intensities (w_σ), for the wind law indicated at the top of the figure, and the value of α shown in the upper left-hand corner. Bottom: The corresponding inverse magnitude of *DF*, plotted as its inverse for easy interpolation.

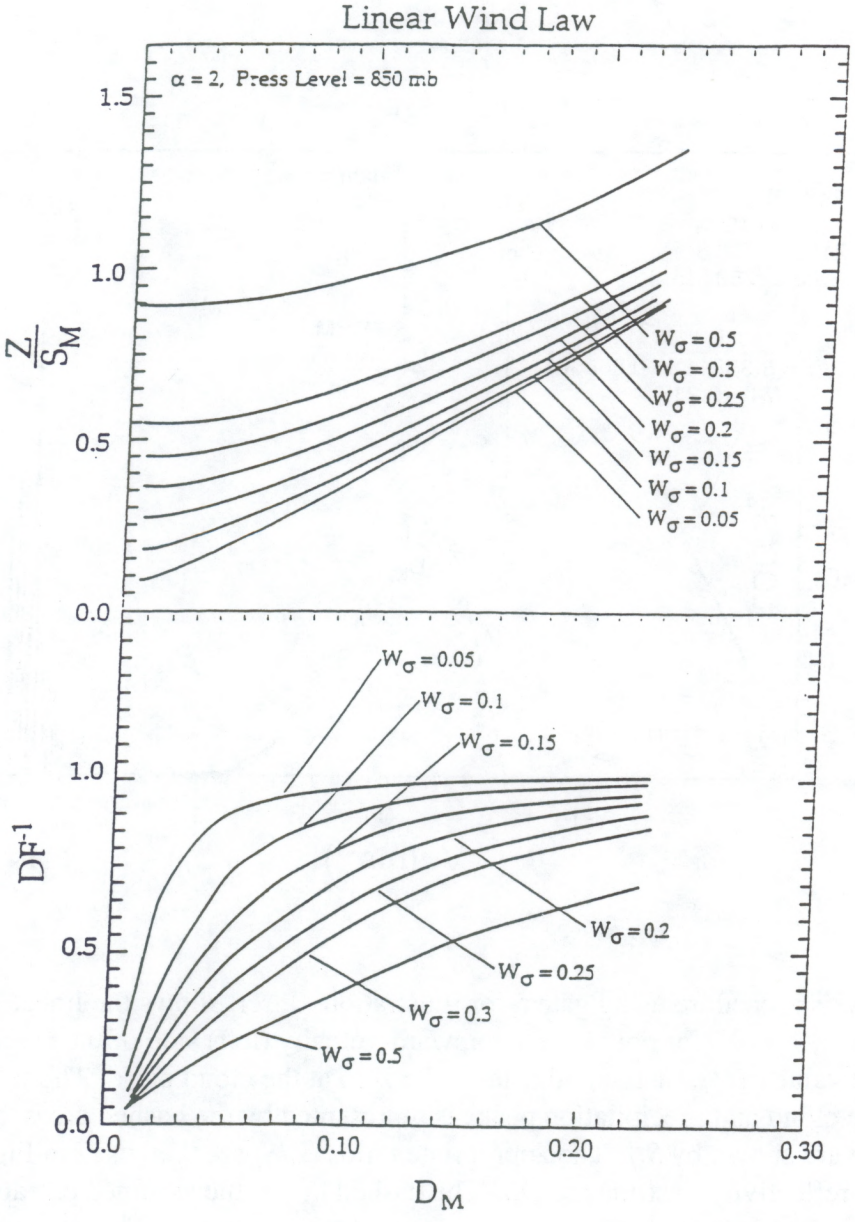

FIGURE 6. Top: Ratio of Z/S_M vs D_M for various turbulence intensities (w_σ), for the wind law indicated at the top of the figure, and the value of α shown in the upper left-hand corner. Bottom: The corresponding inverse magnitude of DF, plotted as its inverse for easy interpolation.

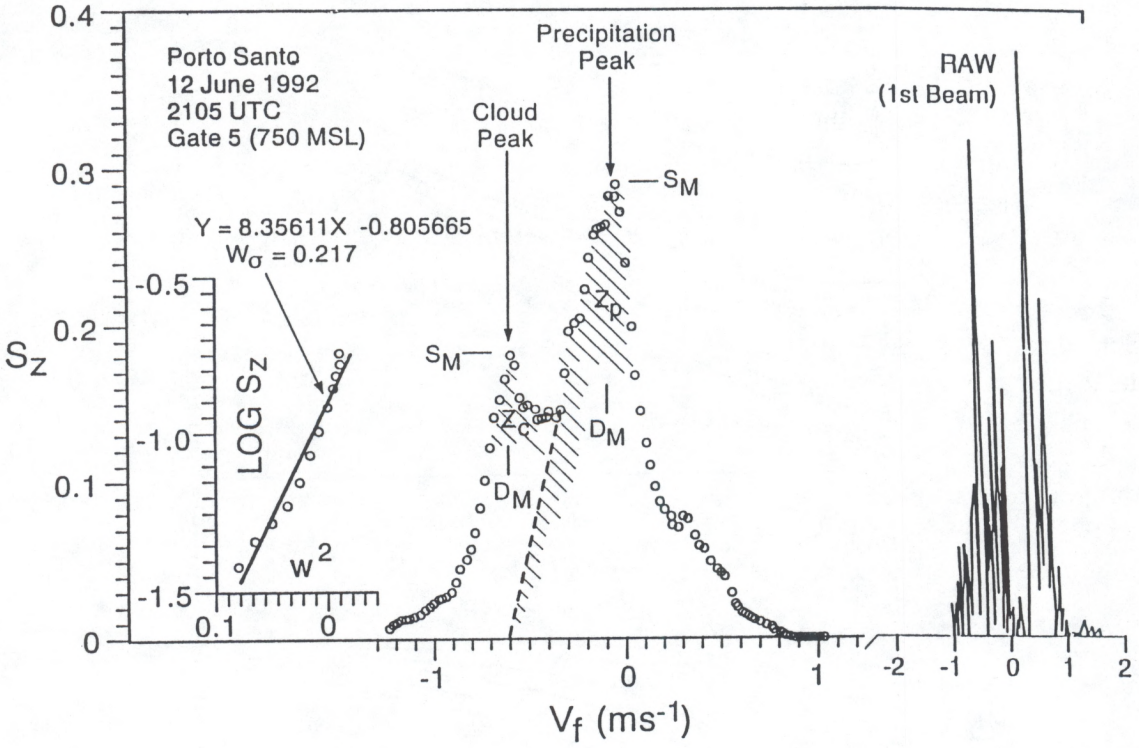

FIGURE 7. Analysis procedure using gate 5 for illustration. Insert shows the linear regression fit of log S_z to w^2 (i.e., Y vs X) for points on the upward-velocity (left) side of the cloud peak to determine a best value of w_σ. w is V_f adjusted to be zero at the cloud peak. The reflectivity factor (Z) for the cloud and precipitation peaks is represented by the hashed areas, and the spectral maxima are shown by S_M. The appropriate ratios (Z/S) are then used in Figs. 3–6. The diameters at the reflectivity maxima are D_M. The dashed line is the assumed extrapolation of the precipitation regime to zero in the area calculation used to calculate Z. The spectral points shown as circles are 100-point averages. For comparison, the first raw spectrum used in the average is shown in the right-hand frame. Note that the cloud and precipitation regimes are clearly separated in the raw data as well as in the averages.

To analyze a measured spectrum, the procedure is as follows:

1. From the velocity *difference* between the precipitation and cloud peaks in the spectrum, find a first estimate of the D_M for the precipitation regime, assuming that the velocity of the cloud peak represents the up/downdrafts in the clear air.

2. Find an optimum value of w_σ from a regression fit of a Gaussian (or exponential) PDF to spectral points on the up-velocity side of the cloud spectral peak (see insert in Fig. 7). The resulting log slope versus V_f^2 (for a Gaussian PDF) will, of course, depend somewhat on the range of points selected for the regression fit. In this example, the regression fit is slightly better for an exponential PDF than for a Gaussian PDF. (Note the curvature of the data points on the regression plot that reduces the correlation coefficient to 0.97, whereas the exponential PDF gives a correlation higher than 0.99. In general, we find that the agreement is not substantially better for one than the other.) To minimize the subjectivity in the selection of the points to be used in the regression analysis, the correlation coefficient should be optimized.

3. Integrate over the spectral peak of the precipitation regime to get its contribution to the total Z measured by the radar (including an extrapolation to zero drop size); then subtract it from the total Z measured by the radar to get the contribution to Z from the cloud regime.

4. Scale off the maximum value of the spectral density of the Z spectrum for the peak of the cloud regime (i.e., the S_M in Fig. 7) and calculate Z/S_M for the cloud regime. Enter this ratio value in the top frame of Fig. 3 or Fig. 5 (for $\alpha = 0$ or $\alpha = 2$) and find the D_M corresponding to the w_σ found in the regression analysis. This is the size scale of the cloud regime.

5. Using the above value of D_M, read the inverse deconvolution factor DF^{-1} from the lower frame of the figure.

6. Having D_M and Z from both regimes, calculate the corresponding LW and FLX from (5a) and (6). Similarly, total number density is found by integration of (2) using (1).

7. Make any higher-order corrections (usually negligible) necessary to account for the effect of the cloud-settling velocity on the velocity difference between the cloud and precipitation spectral peaks.

8. Convert the size scales D_M to the more commonly used mass-median drop size D_0 (e.g., see Gossard 1994) for comparison with data from other sources. [For $\alpha = 0$, $\Lambda = 3.67/D_0 = 6/D_M$, etc., in (1).]

4. DISCUSSION OF THE DATA

Each working profile in this paper consists of an average of 100 raw spectra, giving 10 averaged profiles with a sampling interval of about 20 s throughout the event. Figure 7 shows the first raw spectrum from gate 5 (right) and the first averaged spectrum from the same height. The smoothing and broadening of the averaged spectrum is a result of both turbulent smear and nonstationarity during the averaging interval. Figure 7 also defines many quantities for future use.

The data collection began after the main drizzle event had passed the radar. The time history of the radar reflectivity and the total liquid water from microwave radiometer recordings is shown for gate 5 in Fig. 8. The radar record of liquid water decreases much more quickly after the end of the main drizzle event than does the radiometric record of liquid water. This is reasonable considering the much wider beamwidth of the radiometer. The radiometer averages over a horizontal area of 1600 m^2 at a height of 1 km, whereas the radar beam area is 64 m^2, so the radar's spatial resolution is much greater. The circled points on the liquid water plot represent the liquid in the radar spectra.

The calculated drop-size distributions for $\alpha = 0$ and $\alpha = 2$ are shown for gate 5 in Fig. 9 for (a) the cloud range (left-hand solid line), (b) the drizzle range (center solid line), and (c) the noise level [$\sim D^{-6}$ from (2); right-hand solid curve]. The lower half of Fig. 9 shows the corresponding liquid and flux density spectra for the case of $\alpha = 0$. Figure 10 shows the stacked drop-size distributions for radar gates 2–7, with liquid and flux numerical values listed above each curve. Figures 11–13 show the height profiles of cloud and drizzle liquid, flux, and number density for $\alpha = 0$ and $\alpha = 2$. Figure 14 shows profiles of the mass median diameter and the radar reflectivity factor for $\alpha = 0$. [Note that the median diameter D_0 is related to the modal diameter D_M by $D_0 = (3.67/6)\, D_M$ (Gossard 1994). The median size is that commonly found in the literature. Recall that the modal diameter referred to here is the diameter at the maximum of the reflectivity spectrum.] For most gates, the cloud liquid represents a minimum estimate because the modal diameter was equal to, or less than, 0.04 mm (the smallest diameter reliably resolved), and the smaller the drop size in the cloud regime, the greater the liquid water.

It is evident that total liquid and flux are dominated by the cloud regime. However, the radar reflectivity is dominated by the precipitation (drizzle) regime at gates 5 and 6 (where the main cloud resides). Therefore, radar reflectivity should be a poor indicator of either liquid density or liquid flux under weak precipitation conditions. This has implications for Marshall-Palmer-type relationships.

No aircraft measurements were available in the Porto Santo area at the time of the radar measurements, so aircraft measurements made by Noonkester (1984) in similar stratus clouds off the coast of southern California have been included in Fig. 10. The dotted curve included on the 600-MSL spectrum was recorded by Noonkester at a height of 274 m above cloud base on May 29, 1981, in an air mass he classified as "marine." (Noonkester also reported measurements

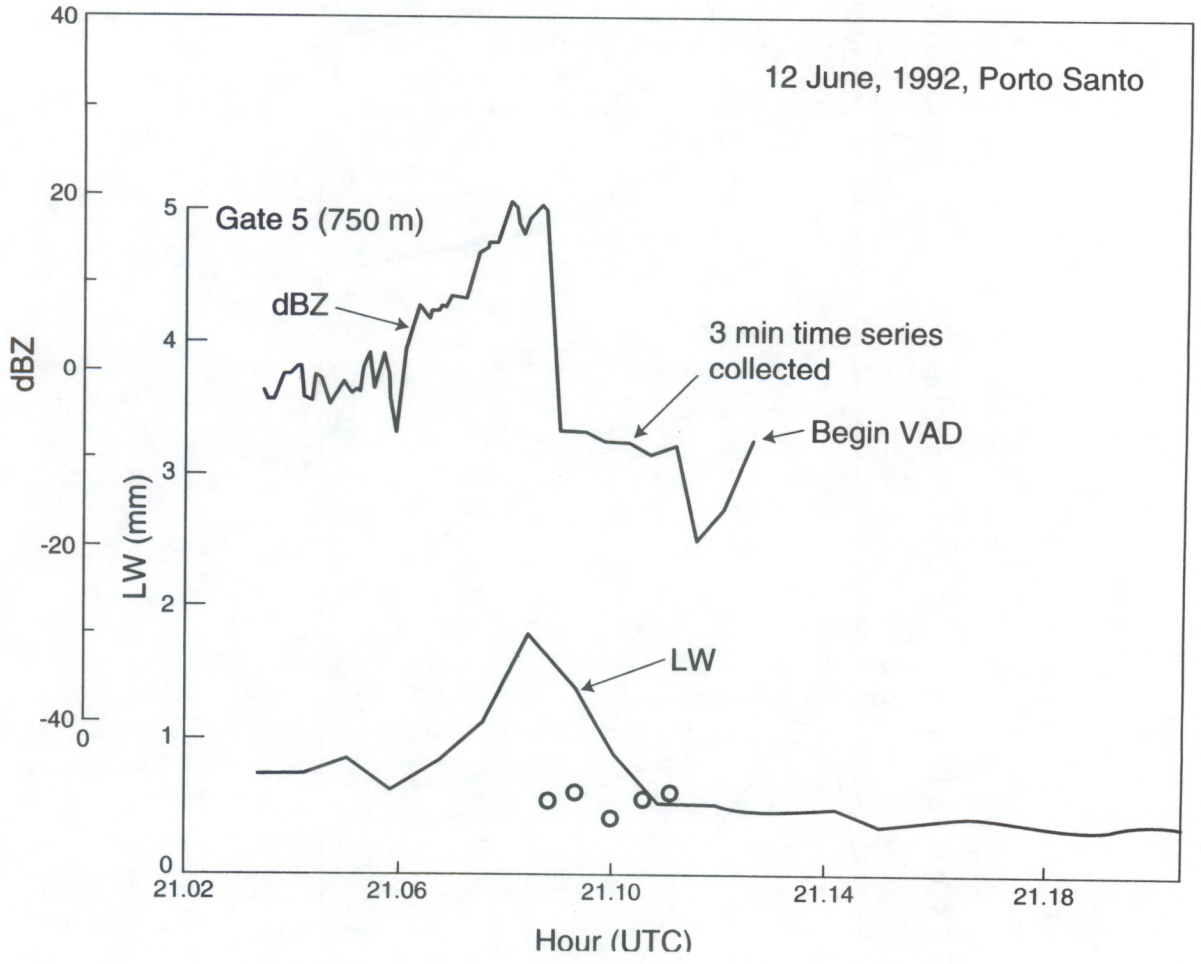

FIGURE 8. Time history of dBZ and radiometric total liquid near the time of the spectra data collection. (This example is for gate 5). Liquid water found from the radar Doppler spectra is represented by circled points. The beamwidth of the radar is 0.5° and that of the radiometer is 2.5°.

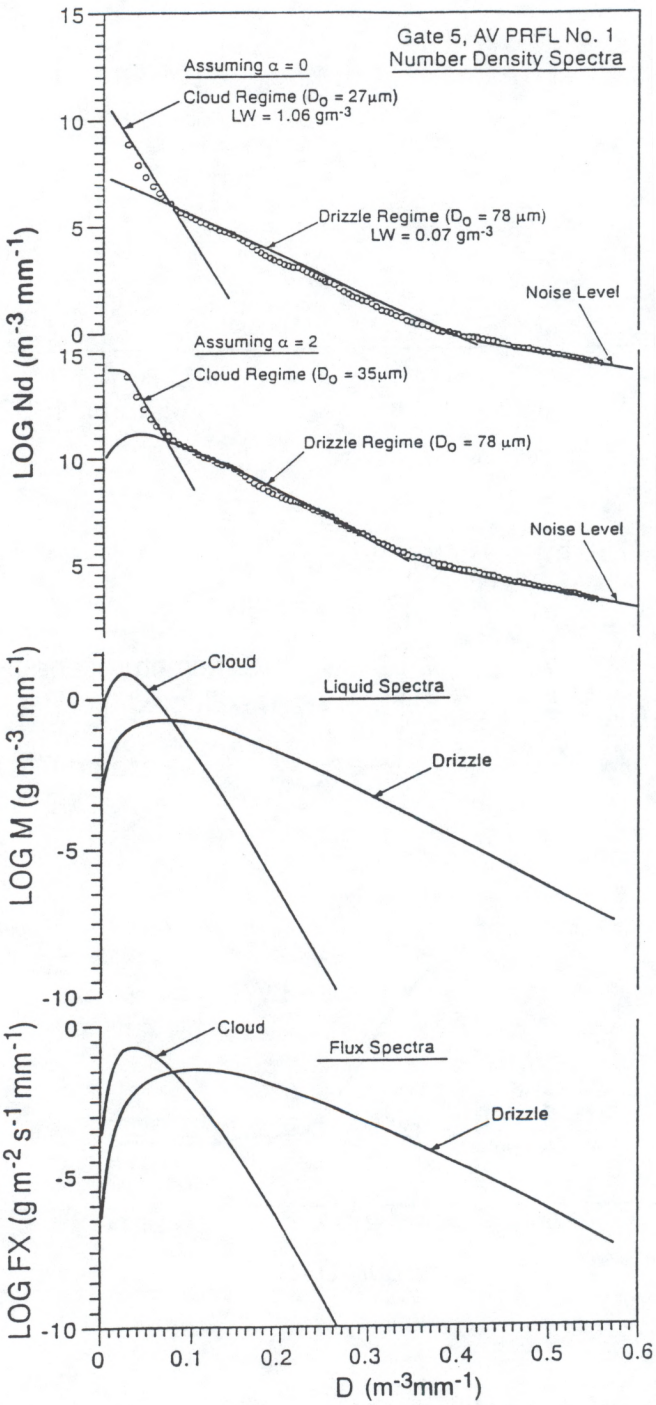

FIGURE 9. Number density, liquid, and flux spectra for the data shown in Fig. 7. Top two curves show the drop-number density assuming $\alpha = 0$ and $\alpha = 2$, and the lower curves show the corresponding liquid and flux densities assuming $\alpha = 0$. The spectra clearly show the cloud regime (left) and a drizzle regime (right). The theoretical regimes, as well as the noise floor, are shown as solid lines on the upper two frames.

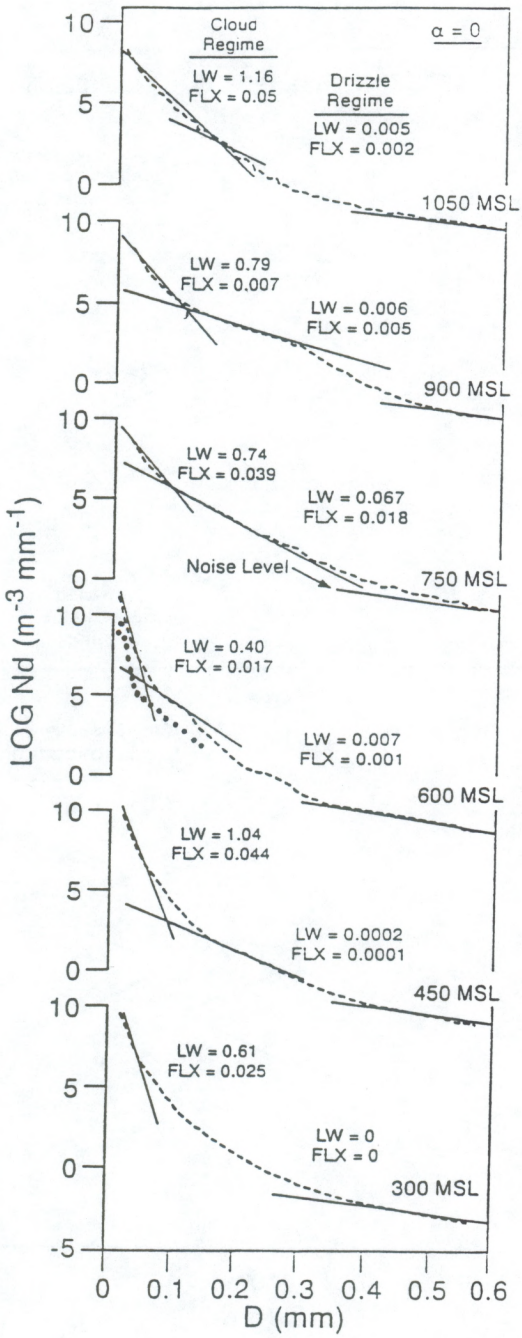

FIGURE 10. Stacked, deconvolved number density spectra calculated for data averaged over the first 100 raw spectra for gates 2–7. Numbers beside the curves are total liquid and flux values for the cloud and drizzle regimes. A spectrum measured by Noonkester (1984) using PMS probes on an aircraft 274 m above cloud base is shown by the dotted curve superimposed on the spectrum at 600 MSL.

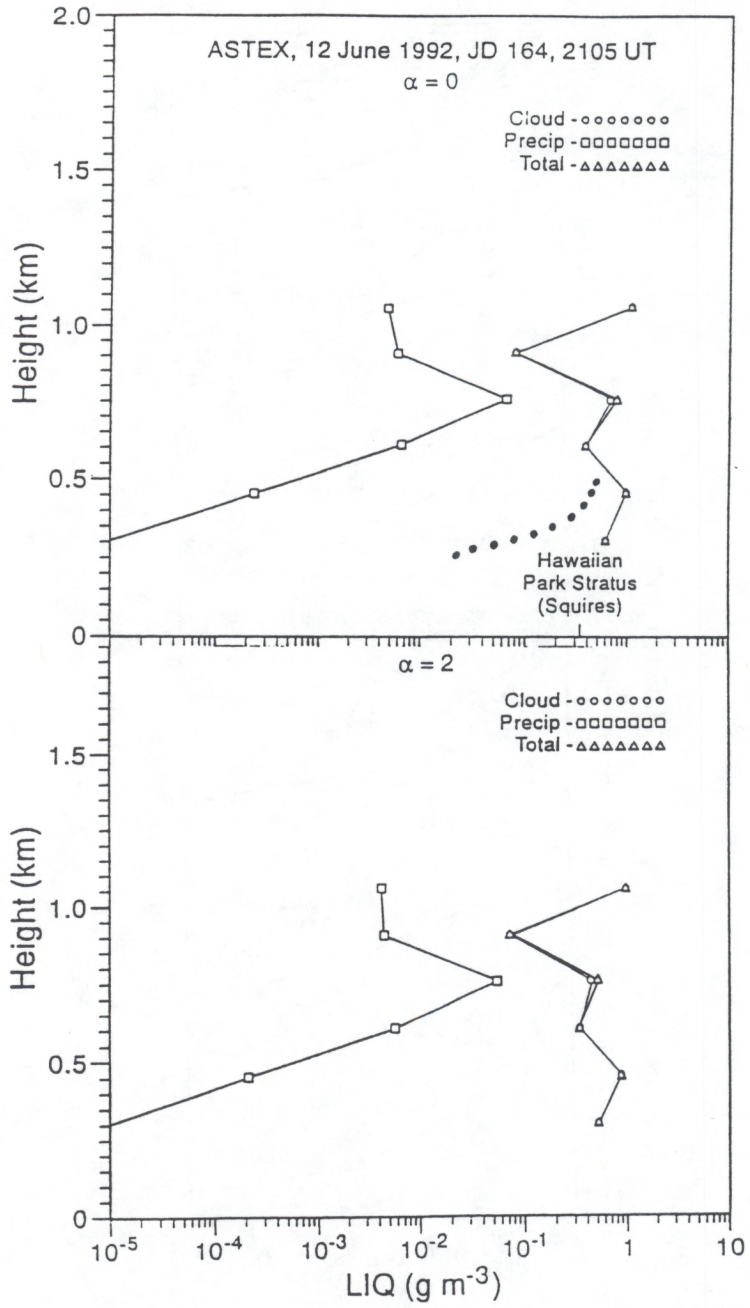

FIGURE 11. Height profiles of liquid for the drizzle regime, cloud regime, and total liquid. Noonkester's (1984) measurements of liquid water near cloud base are shown as dots plotted in the top frame, assuming a cloud base to be at 300 m. Squires' (1958) values of total liquid for Hawaiian dark stratus are indicated on the bottom scale for comparison. Top: $\alpha = 0$. Bottom: $\alpha = 2$.

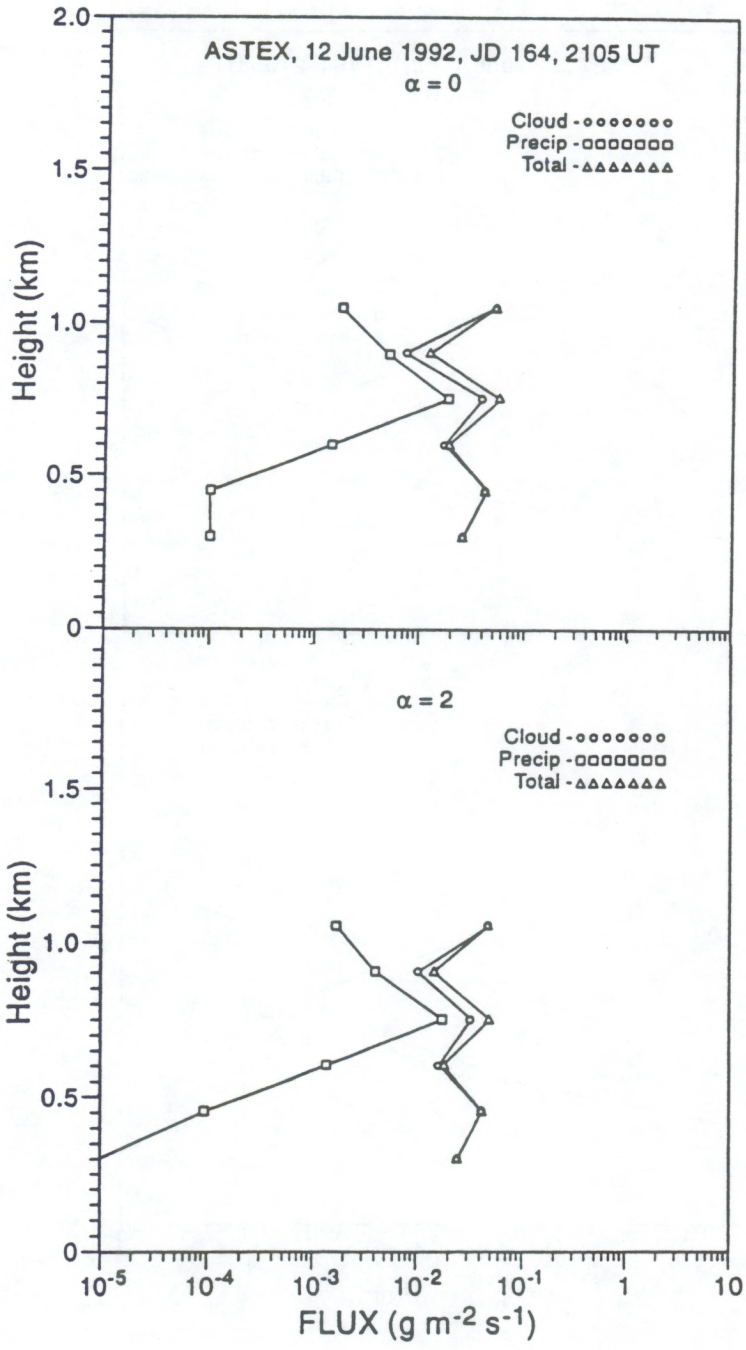

FIGURE 12. Height profiles of flux for the drizzle regime, the cloud regime, and total flux. Average for 100 radar profiles. Top: $\alpha = 0$. Bottom: $\alpha = 2$.

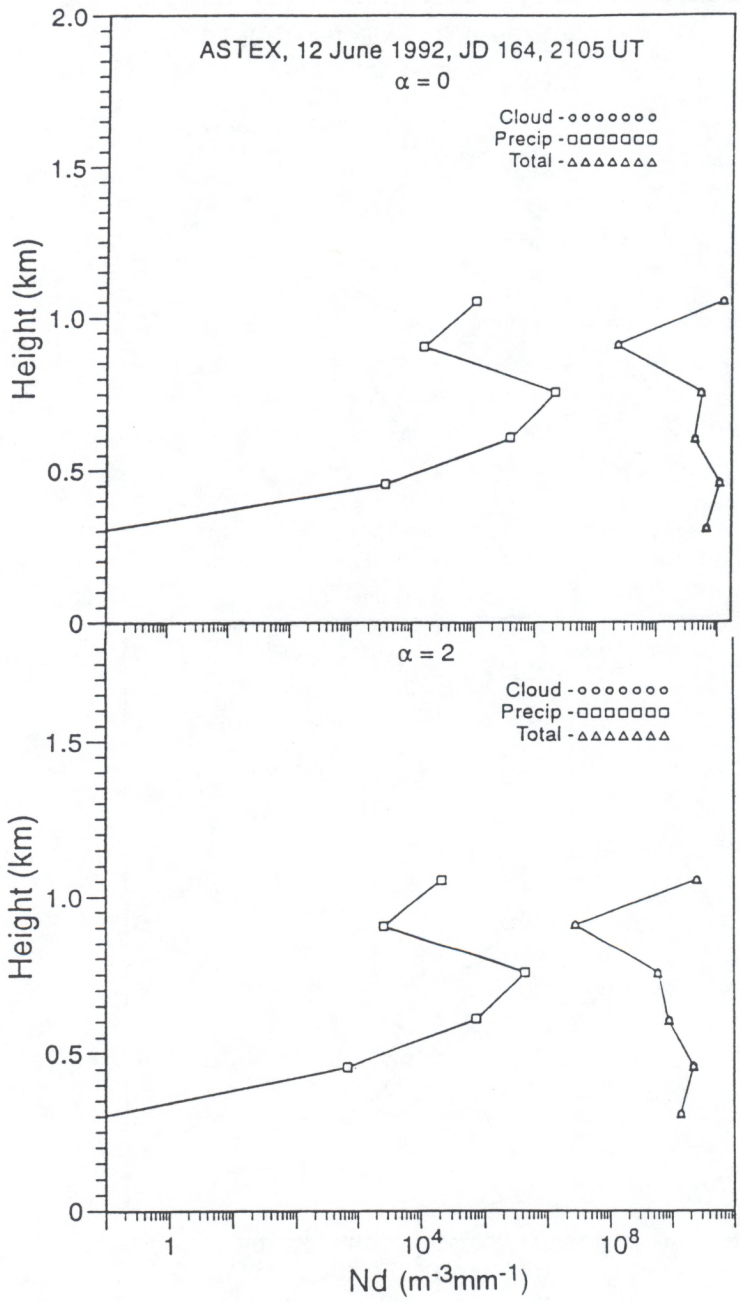

FIGURE 13. Height profiles of drop number in the drizzle regime, the cloud regime, and total number. Top: $\alpha = 0$. Bottom: $\alpha = 2$.

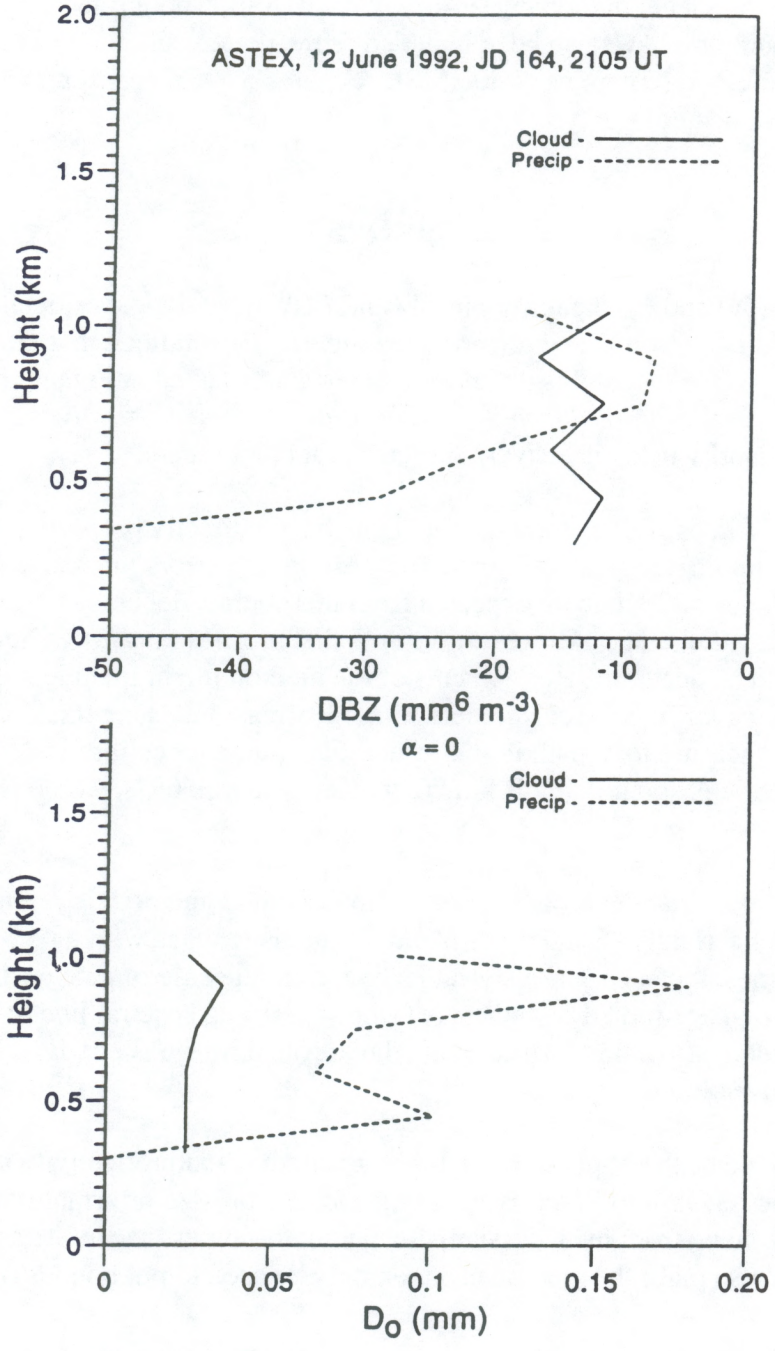

FIGURE 14. Top: Height profiles of radar reflectivity factor for cloud regime and drizzle regime ($\alpha = 0$). Bottom: Height profiles of median drop diameter for cloud and drizzle regimes ($\alpha = 0$).

in August that he classified as "continental.") Noonkester's measurements were made with two spectrometer probes manufactured by Particle Measuring System (PMS), Inc. An ASSP-100 probe measured 32 radius increments in the range $0.23 \leq r < 14.7$ μm, and an OAP-200 probe measured 15 radius increments in the range $14.2 \leq r < 150$ μm. Noonkester's measurements of liquid water near cloud base have also been included as the dotted curve in the top frame of Fig. 11, assuming our cloud base to be at 300 MSL. Squires' (1958) measurements in Hawaiian dark stratus are also indicated.

5. ERRORS

We see from (5a) and (6) that errors in *LW* and *FLX* depend most critically on D_M because it is raised to the third power. It is a noteworthy feature of this technique that D_M depends only on the *ratio* of Z to S_{ZM} [see (4)] and is therefore independent of attenuation and radar calibration. In fact, *the drop size can be inferred from the uncalibrated Doppler reflectivity spectrum*, which is the fundamental quantity most effectively sensed by Doppler radars.

The *LW* and *FLX*, as well as total number density, are directly proportional to Z [see (5a) and (6)], so errors in liquid and flux are directly proportional to errors in radar calibration. Thus, errors of roughly a factor of 2 are to be expected from this source, depending on the care exercised in calibrating the radars. However, we note that profiles of *relative* liquid and flux through clouds should be accurate. Refinements of the method might include incorporating the attenuation of 8-mm waves into the calculation of true Z when clouds are thick and dense, and using radiometers to measure total path liquid to fine-tune the radar calibration. The attenuation to be expected in drizzle is about 0.06 dB km^{-1} (e.g., Kerr 1951, p. 682), which is negligible for many purposes.

Experience shows that the proper identification of cloud and drizzle regimes can be an important source of uncertainty. Sometimes identification is easy, as with gate 5 (upper frame of Fig. 15). At other times, it can be seriously subjective, as in the case of gate 6 (lower frame of Fig. 15), in which the image (noted on the curve) from the strong spectral line of the precipitation appears at an inconvenient location. Minimizing the artificial image is a radar adjustment problem and is readily soluble.

As the size scale of the population becomes small, the cloud reflectivity spectrum departs less and less from the (Gaussian) PDF. Because the cloud drop-size information depends on the departure in spectral shape from the Gaussian, the method becomes inaccurate as the drop size of the population becomes small; the method can then only be used to put bounds on the inferred quantities.

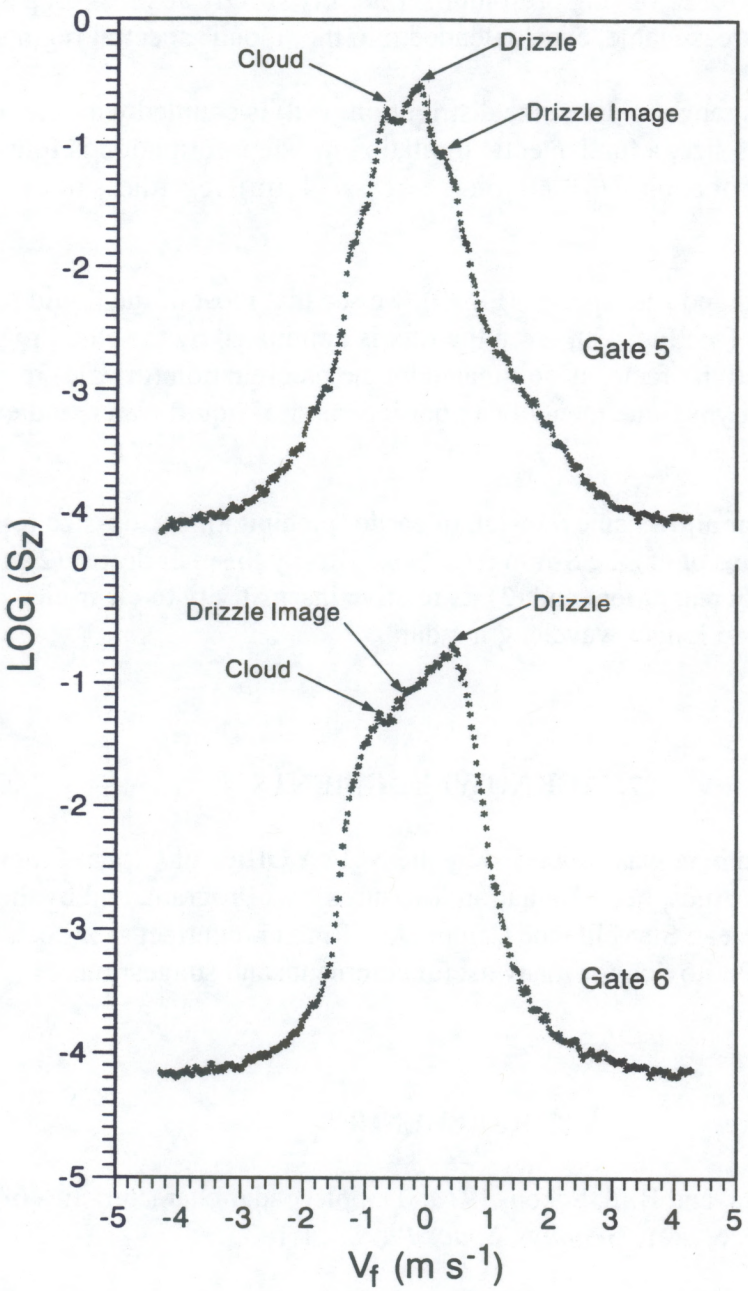

FIGURE 15. Top: Doppler radar spectrum for gate 5, chosen to illustrate a case in which the spectral peaks and regimes are clearly defined. Bottom: Spectrum for gate 6, chosen to illustrate a case in which the spectral regimes are not easily separable, primarily because of artificial images noted on curves. Examples are 100-point-averaged profile data.

6. CONCLUSIONS

1. This technique for retrieving drop-number density spectra at small drop sizes leads to size distributions that are reasonable, even extended into the "cloud" spectral regime.

2. When a Stokes range of drop-size distributions (7d) is coupled with the linear range (7c) of fall velocity versus size, a fundamental limitation in size information is found. This size limit occurs at a diameter of about $D_M = 40$ μm (i.e., $D_0 \approx 24$ μm), regardless of the turbulence intensity.

3. From the liquid and flux spectra (Fig. 9), we see that most of the liquid resides in the cloud regime for all gates (see Fig. 11); even the flux is dominated by the cloud regime. However, the radar reflectivity factor is dominated by the precipitation (drizzle) regime. Therefore, radar reflectivity is fundamentally a poor indicator of liquid water, and even of flux, when the precipitation is light.

4. The 8-mm radar allows an extension of earlier precipitation/drop-size retrievals that used wind profilers because of (1) the 8-mm radar's sensitivity to small drops, (2) its potentially very high spectral-velocity resolution, and (3) its relative insensitivity to clear-air "contamination" possible in longer wavelength radars.

7. ACKNOWLEDGMENTS

The work reported here was supported by the NOAA Office of Global Programs, the Department of Energy's Atmospheric Radiation Measurements Program, and by the Naval Command Control and Ocean Surveillance Center (J. J. Richter, contract monitor). We wish to especially thank Marcia Politovich for many useful comments and suggestions.

8. REFERENCES

Atlas, D., R. C. Srivastava, and R. S. Sekon, 1973. Doppler radar characteristics of precipitation at vertical incidence. *Rev. Geophys. Space Phys.*, 11:1–35.

Currier, P. E., S. K. Avery, B. B. Balsley, K. S. Gage, and W. L. Ecklund, 1992. Use of two wind profilers in the estimation of raindrop-size distribution. *Geophys. Res. Lett.*, 19:1017–1020.

Gossard, E. E., 1988. Measuring drop-size distributions in clouds with clear-air sensing Doppler radar. *J. Atmos. Oceanic Technol.*, 5:40–649.

Gossard, E. E., 1994. Measurement of cloud droplet spectra by Doppler radar. *J. Atmos. Oceanic Technol.*, 3:712–726.

Gossard, E. E., and R. G. Strauch, 1990. The retrieval of drop-size distributions in water clouds from ground-based, clear-air-sensing Doppler radar observations. *Meteor. Rundsch.*, 42:165–173.

Gossard, E. E., R. G. Strauch, and R. R. Rogers, 1990. Evolution of drop-size distributions in liquid precipitation observed by ground-based Doppler radar. *J. Atmos. Oceanic Technol.*, 7:815–828.

Kerr, D. E., 1951. Propagation of short radio waves. Office of Scientific Research and Development, National Defense Research Committee, Dover Publications Inc., 728 pp.

Kropfli, R. A., S. Y. Matrosov, T. Uttal, A. S. Frisch, B. E. Martner, and J. B. Snider, 1994. Studies of radiatively important clouds with 8-mm-wavelength Doppler radar. Preprints, Int'l. Geoscience and Remote Sensing Symposium (IGARSS'94), Pasadena, California. IEEE, 657–659.

Martner, B. E., and R. A. Kropfli, 1993. Observations of multi-layered clouds using K-band radar. Proc., 31st Annual Aerospace Science Meeting, Reno. Amer. Inst. Aeronautics & Astronautics, 8 pp.

Noonkester, V. R., 1984. Droplet spectra observed in marine stratus cloud layers. *J. Atmos. Sci.*, 41:829–846.

Rajopadhyaya, D. K., P. T. May, and R. A. Vincent, 1993. A general approach to the retrieval of raindrop-size distributions from wind profiler Doppler spectra: Modeling results. *J. Atmos. Oceanic Technol.*, 10:710–717.

Rogers, R. R., D. Baumgardner, S. A. Ethier, D. A. Carter, and W. L. Ecklund, 1993. Comparison of raindrop-size distributions measured by radar wind profiler and by airplane. *J. Appl. Meteorol.*, 32:694–699.

Sato, T., H. Doji, H. Iwai, and I. Kimura, 1990. Computer processing for deriving drop-size distributions and vertical air velocities from VHF Doppler radar spectra. *Radio Sci.*, 25:961–973.

Squires, P., 1958. The microstructure and colloidal stability of warm clouds, Part I. *Tellus*, 10:256–261.

Wakasugi, K., A. Mizutani, and M. Matsuo, 1986. A direct method for deriving drop-size distribution and vertical air velocities from VHF Doppler radar spectra. *J. Atmos. Oceanic Technol.*, 3:623–629.

Wakasugi, K., A. Mizutani, and M. Matsuo, 1987. Further discussion on deriving drop-size distribution and vertical velocities directly from VHF Doppler radar spectra. *J. Atmos. Oceanic Technol.*, 4:170–179.

* U.S. GOVERNMENT PRINTING OFFICE 1996-0-774-018/40006